

1 **Xenon LFP Analysis Platform is a Novel Graphical User Interface**
2 **for Analysis of Local Field Potential from Large-Scale MEA**
3 **Recordings**

4 **Arjun Mahadevan¹, Neela K. Codadu², and R. Ryley Parrish^{1*}**

5 1. Department of Cellular and Molecular Biology, Xenon Pharmaceuticals, Burnaby, BC,
6 Canada

7 2. Department of Clinical and Experimental Epilepsy, Institute of Neurology, University College
8 London, Queen Square, London, UK

9 ***Correspondence:** Ryley Parrish; rparrish@xenon-pharma.com

10 **Keywords:** HD MEA, Plotly's DASH, LFP Analysis, Seizures, Scn1a

11 **Abbreviated title:** LFP GUI for MEA recordings

12 **Abstract length:** 347

13 **Manuscript length:** 6184

14 **Number of pages:** 19

15 **Number of figures:** 7

16

17 **Abstract**

18 High-density multi-electrode array (HD-MEA) has enabled neuronal measurements at high
19 spatial resolution to record local field potentials (LFP), extracellular spikes, and network activity
20 with ease. Whilst we have advanced recording systems with over 4000 electrodes, capable of
21 recording data at over 20 kHz, it still presents computational challenges to handle, process,
22 extract, and view information from these large recordings. It can be challenging for researchers
23 to extract and view even a single channel that has more than a billion data points, let alone
24 process a group of channels.

25 We have created a computational method, and an open-source toolkit built on Python, rendered
26 on a web browser using Plotly's Dash for extracting and viewing the data, and creating
27 interactive visualization. In addition to extracting and viewing entire or small chunks of data
28 sampled at lower or higher frequencies, respectively, it provides a framework to collect user
29 inputs, analyze channel groups, generate raster plots, view quick summary measures for LFP
30 activity, detect and isolate noise channels, and generate plots and visualization in both time and
31 frequency domain. Incorporated into our Graphical User Interface (GUI), we also have created a
32 novel seizure detection method, which can be used to detect the onset of seizures in all or a
33 selected group of channels and provide the following measures of seizures: distance, duration,
34 and propagation across the region of interest.

35 We demonstrate the utility of this toolkit, using datasets collected from the 3Brain BioCAM
36 duplex system. For the current analysis, we demonstrate the toolkit and methods with a low
37 sampling frequency dataset (300 Hz) and a group of approximately 400 channels. Using this
38 toolkit, we present novel data demonstrating increased seizure propagation speed from slices of
39 Scn1aHet mice compared to littermate controls.

40 With advances in HD-MEA recording systems with high spatial and temporal resolution, limited
41 tools are available for researchers to view and process these big datasets. We now provide a user-
42 friendly toolkit to analyze LFP activity obtained from large-scale MEA recordings with
43 translatable applications to EEG recordings, and demonstrate the utility of this new graphic user
44 interface with novel biological findings.

45 **1. Introduction**

46 The technology of neuronal data acquisition using high density multi-electrode arrays (HD-
47 MEAs) in tissue and cell cultures has grown dramatically over the past decade (Maccione et al.,
48 2013, Maccione et al., 2015, Ingebrandt, 2015, Müller et al., 2015, Steinmetz et al., 2019, Pault
49 et al., 2022, Maccione et al., 2014). These ever-growing state-of-the-art electrophysiology
50 techniques (Miccoli et al., 2019, Lopez et al., 2018, Stevenson and Kording, 2011) now include
51 commercially available HD-MEA devices that can record extracellular neuronal signals from cell
52 cultures or brain slices on 6 wells simultaneously, where each well consists of 1024 electrodes
53 for a total of 6144 electrodes sampled at 20 kHz or 2304 electrodes for a total of 13824
54 electrodes at 10 kHz (3BrainAG, 2022). A single recording can range in file size from
55 5GB/minute or larger compressed. Several pharmaceutical applications and drug-testing
56 protocols require long-duration recordings from 45 minutes to 90 minutes (Codadu et al., 2019a),
57 which can result in large data files of 350 to 500 GB from these recordings.

58 While electrophysiology and chip technology has progressed at a rapid pace generating high-
59 quality precise neuronal data with a high degree of spatial accuracy, developing data analysis
60 platforms and algorithms exploiting the full potential of the recordings is quite challenging
61 (Mahmud and Vassanelli, 2016, Paninski and Cunningham, 2018). The progress in data analysis
62 pipelines, big data algorithms, flexible analysis platforms to adapt to different techniques, data
63 formats, and research requirements is slowly evolving to handle the large scale of data
64 (Landhuis, 2017). Most applications using high density MEA recordings rely on analysis of
65 high-frequency activity, such as action-potential data, to include useful features, such as spike
66 sorting, clustering, and classification, which has received a lot of attention in the research
67 community, including several open-source architecture toolboxes to view and process the data
68 (Pachitariu et al., 2016, Yger et al., 2018, Lee et al., 2020). Proprietary software and open-source
69 toolboxes that come with the HD-MEA measurement systems can sometimes be restrictive to
70 researchers. While they do provide blackbox-type solutions to spike identification, sorting,
71 generating raster plots and other measures, they may not offer enough customization and
72 adaptability to different methods of viewing and analyzing the data (Bridges et al., 2018).
73 Moreover, while different toolboxes and software platforms provide different functionality, there
74 are benefits and limitations related to the scalability of algorithms for large-scale data, and new
75 paradigms are constantly evolving to exploit the vast potential of these recordings (Mahmud et
76 al., 2012, Diggelmann et al., 2018, Sedaghat-Nejad et al., 2021, Buccino, 2022 January 7).

77 There appears to be many options for analysis of high-frequency activity for large-scale MEA
78 recordings (Peter C. Petersen, 2021, Xin Hu, 2022, Franke et al., 2015, Buccino et al., 2020).
79 However, open-source, user-friendly analysis platforms for visualizing long recordings of LFP
80 collected from HD-MEA systems is limited. From our review of literature and open-source
81 toolboxes, there are limited data-analysis pipelines that are flexible, customizable, and object-
82 oriented methods for processing and visualizing data for low-frequency (0.5 to 300 Hz) LFP
83 activity. This will continue to limit the usefulness of these large-scale MEA recording systems
84 for many electrophysiologists. Nevertheless, there is an increasing number of research labs using
85 HD-MEAs to record LFP activity to understand neuronal network dynamics from cortical slices
86 (Hu et al., 2022, Medrihan et al., 2015, Toader et al., 2013, Ferrea et al., 2012). One available
87 toolbox to view and process MEA data is presented by Bridges et al. (Bridges et al., 2018), built

88 using Python leveraging GPU (Graphics Processing Units) capabilities to view and generate
89 visualization for large MEA data files. In our current work, we present a much different data
90 pipeline with diverse features and summary metrics, that is built on Python, rendered on a
91 browser using Plotly's Dash. This data-analysis pipeline is for band-pass filtered (0.5 to 2048
92 Hz) LFP activity and seizure analysis that is scalable to large datasets, with an interactive GUI
93 for analyzing HD MEA measurements. This GUI includes several features to generate summary
94 measures and plots, and trace LFP activity over time. For people familiar with basic Python, this
95 can also serve as a boiler plate to customize, and add functions and visualization based on
96 individual researchers' analysis requirements.

97 Researchers also require novel ways to track LFP activity over space and time, as calcium
98 imaging is limited by slow kinetics (Wei et al., 2020, Vanwalleghem et al., 2020, Helassa et al.,
99 2016, Tang et al., 2015) and current voltage-imaging techniques have several weaknesses, such
100 as high-bleaching properties (Xiao et al., 2021, Kulkarni and Miller, 2017). Recordings using
101 high-resolution MEA systems offer a new way to explore network communication, with high
102 degree of time and spatial resolution, but require tools to tap into their full potential. Our new
103 data pipeline offers an efficient and easy tool to analyze the spatial and time resolution offered
104 by these MEA systems. We demonstrate the utility of this data pipeline with induction of
105 seizure-like activity and generating example LFP raster plots over time and space, along with
106 example traces from subregions of the brain. This bird's-eye view of LFP activity within our GUI
107 creates a new tool for investigation into novel insight into network dynamics such as how
108 neocortex and hippocampus interact with each other. Furthermore, we demonstrate a novel
109 seizure-tracking approach using the high density of electrophysiological channels with potential
110 to be superior to large-scale calcium imaging to track seizure dynamics. We present data using
111 this analysis tool that shows brain slices from Scn1aHet mice with a deficit in sodium channel
112 NaV1.1, an important channel for interneuron excitability, have more seizure-like events (SLE)
113 than wild-type (WT) littermates in a low Mg²⁺ model. Furthermore, we show novel data that
114 demonstrate an increased seizure-propagation rate in the Scn1aHet mice, likely due to the well-
115 documented decreased firing rates of parvalbumin-positive interneurons in these mouse models
116 (Favero et al., 2018, Tai et al., 2014, Martin et al., 2010). We provide this new python-based
117 software tool as an open-source, customizable solution for analysis and tracking of LFP activity
118 using the 3Brain MEA recording system, but it can easily be adapted to any MEA recording
119 platform. This GUI will also likely be suitable for analysis of large-scale EEG recordings and
120 provide a useful mapping tool for in vivo LFP activity. Our current GUI has a particular utility
121 for analysis of seizure-like activity but can be used for analysis of many other network LFP
122 signals.

123 **2 Methods**

124 **2.1 Ethical approval**

125 All animal handling and experimentation involving animals were conducted following approved
126 protocols according to the guidelines of the Canadian Council on Animal Welfare.

127 **2.2 Slice preparation**

128 Heterozygous *scn1a* knockout (Scn1a(+/-)) mice (Mistry et al., 2014) and WT littermates were
129 used in this study. Heterozygous mice on the 129S6/SvEvTac background (MMRC strain
130 number 037107) are crossed with C57BL/6 mice at The Jackson Laboratory. The pregnant mice
131 are then shipped to Xenon Pharmaceuticals to litter. Pups are then genotyped to determine their
132 genotype as either WT for the *Scn1a* gene (Scn1a++) or heterozygous for the *Scn1a* gene
133 (Scn1a+/-). All mice used in the study were genotyped a second time on the day of euthanasia to
134 reconfirm their genotype. Scn1a and WT mice were used in this study between the ages of P21-
135 P28. Mice were housed in individually ventilated cages in 12 h light, 12 h dark lighting regime.
136 Animals received food and water ad libitum. Mice were anesthetized with isoflurane before
137 being euthanatized by cervical dislocation. Brains were then removed and stored in cold cutting
138 solution (in mM): 3 MgCl₂; 126 NaCl; 26 NaHCO₃; 3.5 KCl; 1.26 NaH₂PO₄; 10 glucose. For
139 multielectrode array recordings, 350 µm horizontal hippocampal sections were made, using a
140 Leica VT1200 vibratome (Nussloch, Germany). Slices were then transferred to a holding
141 chamber and incubated for 1–2 h at room temperature in artificial CSF (ACSF) containing (in
142 mM): 2 CaCl₂; 1 MgCl₂; 126 NaCl; 26 NaHCO₃; 3.5 KCl; 1.26 NaH₂PO₄; 10 glucose. All the
143 solutions were bubbled continuously to saturate with carboxygen (95% O₂ and 5% CO₂).

144 Multi-electrode array recordings were performed on the 3Brain BioCAM DupleX system
145 (Switzerland) using the 3Brain Accura HD-MEA chips with 4,096 electrodes at a pitch of 60µm.
146 Slices were placed onto the electrodes with a harp placed on top to keep the slice pressed down
147 gently to the recording electrodes. Slices were perfused continuously with artificial cerebrospinal
148 fluid (ACSF) that had Mg²⁺ lowered to 25µM to induce epileptiform-like activity. Recordings
149 were obtained from the entire slice, containing both the neocortex and the hippocampus.
150 Experiments were performed at 33–36°C. The solutions were perfused at the rate of 5.0 mL/min.
151 Signals were sampled at 10 kHz with a high-pass filter at 2 Hz.

152 **2.3 Statistics**

153 Statistics were done in GraphPad Prism 9.1.1 (San Diego, CA). Data was analyzed with unpaired
154 Student's t-tests, except for the analysis of seizure duration in Figure 7E, in which a Mann-
155 Whitney test was used due to a significant F-test to compare variances. GraphPad Prism was also
156 used to graph scatter-point data shown in Figure 7. Significance was set at P ≤ 0.05 for all
157 analyses.

158 **2.4 Data analysis and figures**

159 The analysis platform and algorithms used were custom written in Python, including NumPy,
160 pandas, SciPy, and visualizations using Plotly's Dash libraries. The code and sample data files
161 are provided through a [GitHub repository](#)¹. Figures for the manuscript were created using
162 Inkscape 1.1.

163 **2.5 Local field potential (LFP) measures in channel groups**

164 LFP count per second: To detect local field potential from voltage traces, the signal processing
165 library from SciPy in Python is used, specifically the 'scipy.signal.find_peak' function. The

¹ <https://github.com/MicroBrew09/xenon-lfp-analysis>

166 inputs to this function include the ‘threshold’ and ‘width,’ which are received as inputs from the
167 user in the GUI as Threshold (mV) and Time Duration (s) respectively. The ‘find_peak’ function
168 returns the time index of peaks that exceed the minimum threshold value for the minimum
169 specified duration for each individual channel; no maximum limits are set. The sum of count of
170 the peaks for each channel in the group is calculated, which is then summed for all selected
171 channels in the group to get the total LFP count for the group. This is divided by the time range
172 (in seconds) of the signal to return the LFP count/s for the group. The LFP count/s for each
173 channel is just the sum of the LFP count for individual channels divided by the time range. For
174 channels in the measurement file or group of channels selected, active channels have more than
175 20 peaks in the selected time range. The channels are sorted in the decreasing order of LFP
176 activity, and the top 20 most active channels are selected within the group of channels. The LFP
177 count per second is also calculated for the 20 most active channels in the group in certain cases.

$$LFP \text{ count per second} = \frac{\sum \text{Total count of peaks for each channel}}{\text{Time range selected(s)}}$$

178 LFP mean amplitude (mV): For each channel, the absolute voltage amplitude at each peak is
179 calculated, which is used to calculate the average LFP amplitude for each individual channel. For
180 a group of channels, the LFP mean amplitude is the mean of average amplitude of peaks for
181 individual channels. The LFP mean amplitude can also be calculated for the 20 most active
182 channels in the group, rather than include all the channels in the group.

$$LFP \text{ mean amplitude (mV)} = \frac{\sum \text{Average LFP amplitude for each channel in the group}}{\text{Total number of channels in the group}}$$

183 LFP mean duration (s): For each channel, the width of each peak is extracted using ‘properties’
184 in the ‘find_peak’ function, which is used to calculate the average LFP duration (width) for each
185 individual channel in seconds. For a group of channels, the LFP mean duration is the mean of
186 average duration of peaks for individual channels. The LFP mean duration can also be calculated
187 for the 20 most active channels in the group, rather than include all the channels in the group.

$$LFP \text{ mean duration (s)} = \frac{\sum \text{Average LFP duration for each channel in the group}}{\text{Total number of channels in the group}}$$

188 2.6 Seizure-like event (SLE) network measures

189 Maximum distance of spread of SLE: The Euclidean distance from the electrode at which the
190 initiation of SLE is observed in the slice to the furthest point from the initiation point. The row
191 and column number are used as the x and y coordinates respectively. The Euclidean distance
192 between the x, y co-ordinates have no unit. It is multiplied by the electrode spacing in
193 micrometer to get the distance of spread of seizure-like activity in the slice.

$$\text{Maximum distance of spread (\mu m)} = \left[\sqrt{(x_2 - x_1)^2 + (y_2 - y_1)^2} \right] X (\text{Electrode spacing})$$

194 Duration of SLE: This is calculated for each channel in a selected group. The difference between
195 the end time and the start time of the seizure-like event in the selected time window of the
196 ‘Channel Raster (Groups)’ gives the seizure duration for that channel. The mean and maximum
197 duration are calculated for each group from the duration of seizure-like activity of all channels in
198 that group.

$$\text{Duration (s)} = \text{End time of seizure envelop} - \text{Start time of seizure envelop}$$

199 Seizure rate: For the selected time interval in the ‘Channel Raster (Groups),’ the start time, end
200 time of SLE are calculated for all channels in the group. The maximum distance of spread of the
201 SLE is also calculated for that group. The seizure rate is the maximum distance of spread of the
202 SLE divided by the mean difference in the start times of the seizure for each individual seizure.

$$\text{Seizure rate } (\mu\text{m/s}) = \frac{\text{Maximum distance of spread}}{\text{Mean difference in start time of activity in the channels}}$$

203 3 Results

204 The data processing pipeline for LFP activity and seizure analysis consists of three steps starting
205 from the measurement file as shown in Figure 1. A typical measurement file consists of 4096
206 channels recorded for about 50 minutes at a sampling frequency of 10 kHz, in the hdf5 format,
207 the file size is about 250 GB uncompressed. As a first step, channels that overlay the slice are
208 selected based on the desired resolution, and exported using the 3Brain proprietary BrainWave4
209 software. This exported file consists of about 300 to 600 channels with the original sampling
210 frequency, and a reduced file size of 80 GB. The file size and number of channels selected in this
211 step can vary depending on the recording sampling frequency, resolution required for the
212 analysis, and recording time. Second, the extracted channels that overlay the slice from the
213 previous step are down-sampled in Python, this down-sampled file maintains the same data
214 structure and hdf5 format as the original recording, thus has backward compatibility with
215 BrainWave4 software. The down-sampled file is now ready for use with our custom interactive
216 MEA Viewer - Xenon LFP Analysis Platform. The GUI is built in Python using the Plotly’s
217 Dash library, which renders visualizations in a user-friendly web interface. A snapshot of the
218 opening page of the web interface is shown in Figure 2. The analysis platform has the following
219 key functions: 1) MEA Viewer Functions: This includes options to select and view individual
220 channels, generate raster plots for all the channels, apply digital signal processing tools including
221 FFT, low-pass, high-pass, and band-pass filters. 2) Channels Group Functions: This has options
222 to select three different regions or groups of channels, apply peak detection, generate custom
223 raster plots, apply digital signal processing tools, and generate summary measures including LFP
224 count per second, number of active channels, mean LFP amplitude, and mean LFP duration. 3)
225 Seizure Detection and Analysis Functions: This is an unsupervised automatic SLE detection on
226 selected channel groups and analysis of metrics on seizures observed in the slice. Moreover,
227 Python and Plotly’s Dash, which is based on object-oriented programming and reactive
228 callbacks, provide options to customize, change the layout of visualization, analysis methods,
229 summary measures, and data processing algorithms in the GUI, as per the user requirement

230 within each of these functions. The GUI application is either hosted and run on a server or run in
231 the local machine. While running the Python script in the local machine by default the
232 application can be accessed using <http://127.0.0.1:8050/> on a standard web browser.

233 **3.1 MEA viewer functions**

234 A common challenge among researchers using large MEA recording platforms is that it is not
235 easy to explore the raw data. The Xenon LFP Analysis Platform functions are aimed to facilitate
236 exploring the raw data, including viewing entire time-series, apply threshold detection, signal
237 processing tools to individual and groups of channels. The entire platform is built for interactive
238 explorations and analysis, while rendering the visualizations quickly in a few seconds. The time
239 range selection (in Figure 2) is used to load and perform analysis on desired sections of the trace
240 or the entire recording. Selecting channels for analysis is as easy as clicking using the mouse on
241 the green dots that are shown with the slice image in the background (Figure 2). Each point
242 corresponds to the channel location, x and y axis referenced to the original row and column
243 number on the MEA array. Multiple channels can be selected by holding down the shift key
244 while clicking using the mouse. The selected channels automatically load and display for the
245 given time range. Any changes in channel selection, time range selection, or analysis settings
246 dynamically change the analysis measures and output displays. The analysis setting can be used
247 to apply digital low-pass, high-pass, band-pass filters, modify default threshold and duration for
248 peak detection and raster plot generation. All plots are interactive; they can be zoomed in,
249 zoomed out, downloaded as *.png files. Zooming small sections of the time-series in the LFP
250 activity view will automatically generate FFT traces in an adjacent window. These functions are
251 demonstrated in the [supplementary video 1 \(S1\)](#)².

252 Figure 3 shows a sample analysis demonstrating the MEA viewer functions in detail. In this
253 example, 407 channels are exported from the original recording for analysis. The analysis file
254 was down-sampled from 10000 Hz to 300 Hz. The green dots overlay the neocortex, and the
255 electrodes corresponding to the brown dots overlay the hippocampus (Figure 3A). The raster plot
256 in Figure 3B highlights LFP activity in the entire recording. The channels are arranged according
257 to their x, y position in the row and columns from 1 to 4096. The default threshold and duration
258 for LFP activity is 0.07 mV and 0.02 seconds, however the raster can be regenerated for a range
259 of input values by modifying the parameters in the analysis settings (see Figure 2 and [S1](#)),
260 including generating raster after application of low-pass, band-pass, and high-pass filters. Figure
261 3C shows time-series traces from three electrodes (highlighted in Figure 3A); one from the
262 hippocampus displayed in blue, and one from either end of the neocortex displayed in red and
263 aqua, respectively. It is interesting to note the difference in the activity pattern in the three traces
264 at the same instant of time. While Figure 3C show traces for duration of the recording from the
265 selected electrodes, a section of these traces can be selected to view on a faster timescale (Figure
266 3C, AA; Figure 3D), as shown in Figure 3D. The black vertical markers at the top of each trace
267 shows LFP activity detected based on the given threshold and duration. This further highlights
268 the difference in the activity pattern in the different regions of the slice at the same time instance.
269 We can apply digital filters to the traces, for example a 40-150 Hz band-pass filter to view low
270 and high-gamma activity (Figure 3E). We see the blue and red trace have some gamma
271 components, however the aqua trace does not have significant gamma components in the LFP
272 activity. The time traces are interactive; to view spectrum plots (FFT), a small selection of the

² https://youtu.be/Xpg_W8hEmCw

273 trace can be selected which automatically generates the FFT traces adjacent to the time-series
274 traces (as shown in Figure 3E and Figure 3F). The filtered and original traces are usually
275 overlaid, however, to view one or the other, clicking on the legend selects/deselects the trace to
276 view one or both at a time. When digital filters are applied, the amplitude spectrum of the band-
277 pass-filtered and unfiltered (purple) traces are overlayed to show the effect of filtering (Figure
278 3F, unfiltered: purple, filtered: electrode-specific colors).

279 **3.2 Channel group functions:**

280 The channel group functions are aimed at comparing two or three different regions of the slice,
281 and compare LFP activity summary measures, while also generating a raster plot to study
282 difference in activity pattern in different regions. The analysis starts with the ‘Channels Groups’
283 tab (see Figure 2 and [Supplementary video 2 \(S2\)³](#)). Channels groups can be selected by clicking
284 on channels or by using the box or draw tool to select multiple channels at the same time. The
285 groups tab enables selecting channels under three groups (Group1, Group 2, and Group3). The
286 channels for each group are selected under their respective tab. Once respective groups and
287 channels are selected, analysis settings can be modified from the default followed by clicking on
288 ‘Apply Setting and Generate Plots,’ which generates the raster plots and summary measures
289 (Figure 4A and Figure 4B). The measures automatically calculated are also shown in Figure 4B,
290 which include Total LFP count/s, total channels. Channels that have more than 20 LFP activity
291 peaks count in the selected time interval are considered as active channels, and the last three
292 measures are the LFP Count/second, mean amplitude, and mean duration for the top 20 channels
293 in each group. As shown in the summary table, for Group 1 in Figure 4B (bottom), which
294 includes 132 channels in the hippocampus, 83 channels are active, of which only the top 20 are
295 used to compare the mean amplitude and mean duration. When we look at the raster
296 corresponding to the channels in red (hippocampus), there is quite a bit of variability between
297 channels, in the activity count, start times for seizure-like activity. To avoid bias, we select the
298 20 most active channels from each group to calculate and compare mean measures between the
299 groups. Further, the total activity, LFP amplitude, and duration are shown in the summary plot
300 that includes all the channels in the group. The plots and summary measures can easily be
301 regenerated for suitable selection of the time intervals by modifying the time range selection, and
302 channels in each group. The front-end table displays a consolidated summary for all channels in
303 a group, however summary data for each individual channel is automatically generated into an
304 excel file and saved in a results folder for further analysis. The saved analysis file consists of
305 LFP count, mean amplitude, duration, channel number, and group number for each individual
306 channel. This data is overwritten each time the analysis settings change to avoid creating
307 multiple log files. To create a copy, the file can be renamed, or the code can also be modified to
308 save all log files continuously in the results folder.

309 **3.3 Seizure detection and analysis functions**

310 **3.3.1 Seizure detection**

311 Detection and classification of interictal, ictal or SLE can be quite challenging due to different
312 types of epileptiform activity, variability from type of measurement paradigm (4-aminopyridine,
313 low Mg²⁺, low Ca²⁺, high K⁺), and inherent experiment-to-experiment variability (Ghiasvand et

³ https://youtu.be/8T5q2_mpQDg

314 al., 2020, Campos et al., 2018). In the Xenon LFP Analysis Platform, we introduce a simple
315 method to detect SLE using changes in spectral activity and LFP activity in the traces. We found
316 this method quick and easy to apply to many channels (>400 channels) at a time and compare
317 different treatment effects. Moreover, this is efficiently implemented using numpy, scipy, and
318 signal libraries in Python. The steps involved are illustrated in Figure 5.

319 We start with the time-series trace down-sampled to 300 Hz, the first 60 seconds of the trace
320 with no noise, and LFP activity is selected as a reference section of the trace to get a baseline for
321 spectral activity. The spectral magnitude is calculated using the Short-time Fourier Transform
322 (STFT), with a few variable parameters that can be set or standardized in the analysis platform,
323 including length of time segment, window, and overlap points, which is shown in Figure 5B.
324 Two sliding windows of dimension 30 datapoints and 500 datapoints are applied to the spectral
325 activity peaks and LFP activity peaks independently, to detect regions of continuous seizure-like
326 activity and time regions of no activity (Figure 5C and Figure 5D). This has a few parameters
327 that can be standardized based on the experiment paradigm. In the examples discussed we use 6
328 standard deviations from the baseline spectral magnitude to detect high spectral activity and 0.07
329 mV voltage threshold, 0.02 s duration for LFP activity. The sliding window length (30 X 1 and
330 500 X1) and cutoff threshold parameter for automatically detecting spectrally active time regions
331 post windowing can also be standardized. Once we have the time points of continuous spectral
332 activity and LFP activity, we use overlapping points of both spectral activity and LFP activity to
333 detect the seizure envelop. In general, the start of SLE is primarily detected when the spectral
334 activity exceeds 6 standard deviations from the baseline and has continuous spectral and LFP
335 activity for a minimum of 10 seconds. This again can be modified based on the experiment
336 paradigm. If some seizures are closely spaced, parameters can be changed to a different value
337 based on user preference. Once we have the seizure envelop with start and end times, we use this
338 to further calculate the rate of seizure spread, distance of spread of seizure within a region of a
339 slice using the group selection as discussed in the next section. This being an unsupervised
340 method, and the variability of the nature of seizure-like activity in different regions of the tissue
341 and between experiments, this may require manual verification by selecting a few channels and
342 checking if the automatic envelop detect has good accuracy. We noticed that when the signal to
343 noise ratio is high, and when clear LFP activity and spectral activity is detected, the algorithm
344 performs well, but may need some adjustments to the parameters when the signal to noise ratio is
345 low or LFP activity is not clearly differentiable.

346 **3.3.2 Seizure analysis**

347 The channel group raster is required to perform the seizure detection and analysis. Each group
348 has a separate tab ([Supplementary video 3 \(S3\)](#)⁴) under which individual channels can be
349 selected to view seizure-like activity highlighted by the envelop (Figure 6A). Figure 6B
350 demonstrates the raster plot for three different groups. Using the raster, a region can be selected
351 with a potential SLE, as shown in Figure 6B (non-grey section), to generate summary measures
352 and a visual of the channels that have a SLE within the selected section (Figure 6C). The channel
353 dots highlighted in red are channels in the respective group that have a SLE, the blue dots are

⁴ <https://youtu.be/8XhgCPpj3Ek>

354 channels that did not participate in the SLE, while the grey dots have not been selected. The time
355 interval shown in the summary table in Figure 6C is the selected time interval in the raster plot
356 (Figure 6B -non-grey section). The distance, duration, and seizure rate are calculated from the
357 start and end times of seizure envelop in each of the channels in the group for the selected
358 (zoomed in) seizure.

359 Three metrics are calculated from the seizure envelop for all channels in the group: distance of
360 spread, duration, and seizure propagation speed. The spatiotemporal origin of the seizure within
361 a group is identified as the channel that first had spectral activity above the set threshold, and this
362 timestamp and the location of the channel is used to further calculate the distance and rate of the
363 seizure spread. For example, in Figure 6C, it is the maximum distance from the green dot to the
364 furthest red dots. If more than one channel is highlighted green, then they have similar start
365 times, and the maximum distance from each point is calculated to find the overall maximum
366 distance. The blue dots do not have a seizure-like event and are not included in the calculation.
367 The x, y position on a 64X64 grid places the channels at 1 unit dimension from each other. The
368 array spacing in micrometer is multiplied by the distance and seizure rate to get the final measure
369 in micrometer and micrometer/second respectively.

370 We next used this seizure tracking function to examine if slices from Scn1aHet mice, which are
371 heterozygous for NaV1.1, have an altered phenotype in the low Mg²⁺ model of epilepsy. The
372 example raster plots demonstrate a likely difference in number of seizure-like events between
373 WT littermates and the Scn1aHet animals (Figure 7A). Further analysis revealed that the
374 Scn1aHet mice do have significantly more seizures than the WT littermates over the course of
375 the 50-minute recording (Figure 7B). Furthermore, we found that the start time to first seizure-
376 like event was significantly sooner in the Scn1aHet animals compared to controls, further
377 demonstrating an increased seizure phenotype in animals with a deficit in NaV1.1 expression
378 (Figure 7C). Using our novel seizures tracking algorithm within our GUI, we compared the
379 speed of seizure propagation in slices from control mice verses the Scn1aHet mice. Interestingly,
380 this analysis demonstrated a significantly faster rate of seizure propagation in brain slices from
381 the Scn1aHet mice compared to control (Figure 7D). There was no significant difference found
382 in the duration of the seizures between the control and Scn1aHet mice (Figure 7E). This data
383 demonstrates novel phenotypic feature of the Scn1aHet mice, a decreased time to the appearance
384 of the first seizure-like event, and an increased rate of seizure spread through the tissue, likely
385 due to deficits in feed-forward inhibition provided by the somatostatin and parvalbumin
386 interneurons (Parrish et al., 2019, Cammarota et al., 2013, Trevelyan et al., 2007). These new
387 analysis features provided by the Xenon LFP Analysis Platform provide new and exciting ways
388 to understand phenotypic differences in transgenic animals, understand how pharmacology
389 impacts neuronal network activity over space and time, and is customizable to fit any
390 researcher's needs.

391 **4 Discussion**

392 The Xenon LFP Analysis Platform aims to produce a lightweight interactive application with
393 high-quality visualization rendered on a web browser, using open-source libraries (Python &
394 Plotly's Dash) that can be standardized to an individual's research requirements. In the examples
395 shown in the results section, we provide a snapshot of simple visualization and signal processing

396 tools, however this can be expanded and customized to include additional features as per the
397 users' requirements by building simple data analysis models/functions and rendering them using
398 callbacks in Plotly's Dash. The data models with Xenon LFP Analysis Platform enable creating
399 summary measures for comparisons, and visualizations on the browser, creating an interactive
400 toolbox for viewing millions of datapoints at a time, to extract meaningful results and
401 conclusions from the measurements. Furthermore, the application is scalable to larger datasets,
402 with the ability to build functions that selectively read from small chunks of data from the hdf5
403 array rather than load the entire dataset into memory for rendering on the browser. However, it
404 should be noted one of the drawbacks of hdf5 files to store HD-MEA data is that using single
405 dimension large arrays to store data makes indexing and selectively reading channels very
406 inefficient and difficult to parallelize (Dragly et al., 2018, Rossant, 2016b, Rossant, 2016a). Most
407 HD-MEA measurement systems use the hdf5 files system to record/write data to disk, which has
408 its advantages for portability of data, but limits data analysis pipelines to parallelize signal
409 processing tasks on distributed systems or multicore processors and GPUs. Some cases require
410 reading the entire array to memory for extracting a group of channels to apply a band-pass filter
411 or Fast Fourier Transforms (FFT). The current working file size on the Analysis Platform is
412 limited by local system RAM. Future work can extend the current platform to include a data
413 pipeline to work with larger files of 250 GB or more exceeding the system memory, using
414 parallel computing algorithms for signal processing and visualization tasks including filtering,
415 FFT analysis, spike sorting on a larger scale, which is a developing research area for
416 computational neuroscience that requires more exploration (Jonathan W. Pillow, 2019, Street,
417 2021).

418 The spatiotemporal resolution of HD-MEA recordings on tissue slices provides high-quality
419 data, while also presenting big data challenges in visualization and analysis, including extracting
420 meaningful reproduceable results. This can further be complicated when testing long-duration
421 drug protocols to include multiple compounds at different concentrations resulting in terabytes of
422 data that can become overwhelming to analyze and compare (Perkel, 2018). There is always a
423 need for simple data pipelines and new analysis platforms that are open source, user friendly,
424 scalable, and portable that can produce repeatable analysis results for ease of comparison
425 between paradigms and datasets (Sejnowski et al., 2014, Mouček et al., 2014). Standardization of
426 analysis tools to compare different drug protocols is key to make sense of terabytes of data
427 collected using different compounds, concentrations, and drug-treatment effects (Sobolev et al.,
428 2014). The LFP Analysis Platform enables this by setting up standard functions with
429 customizable parameters to generate raster plots and LFP metrics, this includes unsupervised
430 methods to detect seizure-like activity. There are three key groups of measures: 1) summary
431 measures relating to all channels in each recording, 2) metrics relating to channel groups, and 3)
432 seizure-like event measures tracked for selected regions in the raster plots for channel groups. In
433 the first step, LFP activity raster and activity count for all active channels are summarized in
434 'LFP Detection (All Active Channels)' tab (Figure 2). This data is not saved and is just rendered
435 on the browser for viewing, which may be useful to quickly review the recording. This is also
436 linked to the selected time range and analysis settings, including threshold, duration, and digital
437 filter parameters. In the second step, channel groups or select regions of the slice may be selected
438 along with a specific time range to generate custom raster plots, along with metrics like the

439 number of active channels, LFP count, mean LFP amplitude, mean LFP duration ('Channel
440 Raster (Groups)'). As shown in the results section, this is particularly useful to compare different
441 regions of the slice, or different time regions within a recording for drug treatment effects. In
442 addition to viewing, all measures for individual channels in each group are automatically saved
443 as a csv file in the background for further analysis. In the third step, the raster generated in step
444 two can be used to select specific time points of activity to view and analyze LFP and SLE
445 activity (Figure 5). These measures track network activity based on seizure envelops, start times,
446 and end times. This being an unsupervised method, and due to the variability in measurement for
447 different slices and protocols, user intervention may be required in some cases to check the
448 activity envelop, and careful selection of activity regions in the raster plot. It is our hope that
449 making this analysis platform fully open source will allow others to add functions that enhance
450 its utility for all and aid in addressing limitation of this current GUI, such as aspects of the
451 analysis requiring some user intervention and finding work arounds to streamline analysis of
452 even larger data sets.

453 With the advent of larger recording systems, allowing for up to 6 slices and over 1000 channels
454 per slice during a single recording session, tools like this GUI are timely. These new systems will
455 allow for immense screening of transgenic animals to elucidate aberrant network behavior
456 (Mackenzie-Gray Scott et al., 2022) and large-scale drug screening of biological tissue.
457 Furthermore, there is need to understand with epilepsy and other disorders how different brain
458 regions interact with each other when challenged in media that induces increased network
459 activity or when stimulated electrically or optogenetically (Cela and Sjostrom, 2020, Rafiq et al.,
460 2003, Codadu et al., 2019b). While we now have the recording platforms to facilitate these
461 research needs, we are still limited by analysis tools, and here we directly address some of these
462 needs in our GUI and set important groundwork for further developments within this platform.
463 We also perceive that this GUI will be useful in other large-scale electrophysiological recording
464 systems where the researcher wants to understand interactions between LFP activity at different
465 recording sites over space and time. For example, it would be particularly interesting to visualize
466 multichannel human EEG recordings within the framework of this GUI, which could provide
467 easy and efficient visualization of channel recruitment during various behavioral states with the
468 current built-in features and custom additions.

469 Overall, the Xenon LFP Analysis Platform introduces a standard approach to analyze large HD-
470 MEA recordings, using high-quality visualization rendered on a browser, simple algorithms, and
471 metrics, with lot of customizable features and options for researchers. We demonstrate the utility
472 of this new analysis platform with ex vivo data and demonstrate a novel finding in a low Mg²⁺
473 model of epilepsy from Scn1aHet animals. Slices from the Scn1aHet animals display an
474 increased rate of seizure propagation compared to slices from WT littermates. Using hundreds of
475 channels to map spreading activity such as seizures adds another important tool in the hands of
476 neuroscientists and will complement low-resolution traditional imaging techniques, such as Ca²⁺
477 imaging and dye-based voltage imaging. We hope this GUI will serve as a tool for collaborative
478 work between research labs to contribute add-ons and share results and findings.

479 **Data availability statement:** The raw data supporting the conclusions of this article will be
480 made available by the authors, without undue reservation.

481 **Acknowledgments:** We would like to thank the entire Xenon family for their support of this
482 work.

483 **Author contributions statement:** RP conceived this work. AM, NC, and RP designed the
484 computational methods. AM wrote the code and designed the visualizations. RP collected the
485 data. AM and RP analyzed the data. AM and RP wrote the manuscript. AM, NC, and RP edited
486 and approved the final draft.

487 **Funding:** This project was funded by Xenon Pharmaceuticals.

488 **Conflict of interest statement:** Arjun Mahadevan and R. Ryley Parrish are employees of Xenon
489 Pharmaceuticals Inc. and may hold stock or stock options in the Company. Neela K. Codadu
490 declares no conflict of interests.

491 **Figure legends**

492 **Figure 1: High-density multi-electrode array (HD MEA) data-analysis pipeline.** The data
493 processing for LFP activity detection and network analysis starts by selecting a group of about
494 600 channels that overlay the slice or region of interest, which are exported from the original
495 hdf5 measurement raw file (4096 channels, sampled at 10 kHz) to a reduced hdf5 file. This
496 reduced file is further down sampled from 10 kHz to a desired frequency. This will be the
497 working hdf5 file for the Xenon LFP Analysis Platform. [3Brain Logo: © Copyright 3Brain AG,
498 Python Logo: © Copyright Python Software Foundation, Plotly's Dash Logo: © Copyright
499 Plotly]

500 **Figure 2: Snapshot of the analysis GUI features.** A view of the analysis GUI which is
501 rendered in a html browser built on Python using Plotly's Dash. The GUI has several interactive
502 features from individual and group channel selection, low-pass, high-pass, and band-pass
503 filtering, viewing entire trace or a small section of the trace, Fast Fourier Transformation (FFT)
504 of sections from selected traces, customized raster plots, small groups of channels, and
505 generation of group summary measures.

506 **Figure 3: Example visualizations generated from the GUI including raster plots, time-**
507 **series traces, LFP activity peaks, and time frequency transformations.** (A) 407 channels
508 selected for this analysis representing the MEA sensor spatial array, covering both the neocortex
509 and the hippocampal regions. (B) Raster plot for all the channels in the working file irrespective
510 of brain regions for a selected time range, demonstrating time points of when the activity occurs
511 in the slice. (C) Three selected traces, the blue trace being from the hippocampal region, the red
512 trace being from one end of the neocortex, and the aqua trace being from the other end of the
513 neocortex. (D) Zoomed in view of the first seizure (the region bracketed in (C) as AA), with the
514 black dashes showing a peak find function within the GUI. (E) This demonstrates the ability to
515 plot filtered traces along with the raw traces. (F) The amplitude frequency transformations for
516 the traces in (D) and (E) (band-pass filtered), the filtered FFT spectrum for each is shown in
517 purple.

518 **Figure 4: Channel groups and raster plot can be generated to visualize LFP activity in**
519 **different regions of the slice.** (A) Sensor locations corresponding to three different regions
520 selected for analysis and the region-specific raster plots. Group 1 being the hippocampus, whilst
521 group 2 and 3 each being one half of the Neocortex. (B) Summary plots and measures that can be
522 generated within the analysis platform.

523 **Figure 5: Simple and fast unsupervised seizure detection method.** (A) The raw trace from the
524 recording down sampled to 300 Hz frequency for a sample channel. (B) Spectral activity
525 calculated from the Short-time Fourier Transform using Hanning Window, for a time window
526 length of 1 second, with no overlap. (C) LFP activity detected using a threshold of 0.07 mV and
527 0.02 s, followed by applying two sets of sliding windows (length 30 datapoints, and 500
528 datapoints) to detect time regions of continuous activity. (D) Spectral activity detected when the
529 magnitude is greater than 6 standard deviations from the reference spectrum. The spectral
530 activity is also passed through two sliding windows to detect regions of continuous spectral
531 activity. (E) The overlapping regions of LFP activity and spectral activity of 10 seconds or more
532 are used to identify the seizure envelop. The start of seizure is primarily identified using the time
533 point when the spectral activity is greater than 6 standard deviations from the baseline.

534 **Figure 6: Seizure activity tracking over space and time.** (A) Seizures in individual channels in
535 a group are automatically detected, and their respective start and end times can be tracked across
536 channels in that group. (B) Regions of the raster between time intervals can be selected as
537 demonstrated to generate seizure maps of selected brain regions within the interval. (C) Seizure
538 map for the time interval selected and channels in the group, including initiation sight of the
539 seizure, maximum distance the seizure spread from the initiation point, duration of the seizure,
540 and the rate of seizure spread across the tissue.

541 **Figure 7: Scn1aHet mice have an altered seizure pattern in the low Mg²⁺ model.** (A)
542 Example raster plots from control slices and slices from Scn1aHet mice. (B) Scn1aHet have
543 significantly more SLE than littermate controls (unpaired t-test, p = 0.04, n = 7-9). (C) From the
544 slices that displayed SLE, Scn1aHet demonstrated a significant increase in time to first seizure
545 compared to littermate controls (unpaired t-test, p = 0.006, n = 5-7). (D) SLE from the Scn1aHet
546 propagate significantly faster than seizures in the littermate controls (unpaired t-test, p = 0.008, n
547 = 10-14). The first two seizures from the slices that had SLE were used in this analysis. (E)
548 Seizure duration was not different between Scn1aHet and littermate controls (Mann-Whitney
549 test, p = 0.66, n = 10-14).

550 5 References

- 551 3BRAINAG. 2022. *Hyper CAM Alpha* [Online]. Available:
552 <https://www.3brain.com/products/multiwell/hypercam-alpha> [Accessed March 03 2022].
- 553 BRIDGES, D. C., TOVAR, K. R., WU, B., HANSMA, P. K. & KOSIK, K. S. 2018. MEA Viewer: A high-
554 performance interactive application for visualizing electrophysiological data. *PLOS ONE*, 13,
555 e0192477.
- 556 BUCCINO, A., GARCIA, S., & YGER, P. 2022 January 7. Spike sorting: new trends and challenges of the era
557 of high-density probes. *OSFPrePrints*.
- 558 BUCCINO, A. P., HURWITZ, C. L., GARCIA, S., MAGLAND, J., SIEGLE, J. H., HURWITZ, R. & HENNIG, M. H.
559 2020. Spikelinterface, a unified framework for spike sorting. *eLife*, 9, e61834.
- 560 CAMMAROTA, M., LOSI, G., CHIAVEGATO, A., ZONTA, M. & CARMIGNOTO, G. 2013. Fast spiking
561 interneuron control of seizure propagation in a cortical slice model of focal epilepsy. *J Physiol*,
562 591, 807-22.
- 563 CAMPOS, G., FORTUNA, A., FALCAO, A. & ALVES, G. 2018. In vitro and in vivo experimental models
564 employed in the discovery and development of antiepileptic drugs for pharmacoresistant
565 epilepsy. *Epilepsy Res*, 146, 63-86.
- 566 CELA, E. & SJOSTROM, P. J. 2020. A Step-by-Step Protocol for Optogenetic Kindling. *Front Neural Circuits*,
567 14, 3.
- 568 CODADU, N. K., GRAHAM, R. T., BURMAN, R. J., JACKSON-TAYLOR, R. T., RAIMONDO, J. V., TREVELYAN,
569 A. J. & PARRISH, R. R. 2019a. Divergent paths to seizure-like events. *Physiol Rep*, 7, e14226.
- 570 CODADU, N. K., PARRISH, R. R. & TREVELYAN, A. J. 2019b. Region-specific differences and areal
571 interactions underlying transitions in epileptiform activity. *J Physiol*, 597, 2079-2096.
- 572 DIGGELMANN, R., FISCELLA, M., HIERLEMANN, A. & FRANKE, F. 2018. Automatic spike sorting for high-
573 density microelectrode arrays. *Journal of neurophysiology*, 120, 3155-3171.
- 574 DRAGLY, S.-A., MOBARHAN, M. H., LEPPERØD, M., TENNØE, S., FYHN, M., HAFTING, T. & MALTHE-
575 SØRENSEN, A. 2018. Experimental Directory Structure (Exdir): An alternative to HDF5 without
576 introducing a new file format. *bioRxiv*, 249979.
- 577 FAVERO, M., SOTUYO, N. P., LOPEZ, E., KEARNEY, J. A. & GOLDBERG, E. M. 2018. A Transient
578 Developmental Window of Fast-Spiking Interneuron Dysfunction in a Mouse Model of Dravet
579 Syndrome. *J Neurosci*, 38, 7912-7927.
- 580 FERREA, E., MACCIONE, A., MEDRIHAN, L., NIEUS, T., GHEZZI, D., BALDELLI, P., BENFENATI, F. &
581 BERDONDINI, L. 2012. Large-scale, high-resolution electrophysiological imaging of field
582 potentials in brain slices with microelectronic multielectrode arrays. *Front Neural Circuits*, 6, 80.
- 583 FRANKE, F., QUIAN QUIROGA, R., HIERLEMANN, A. & OBERMAYER, K. 2015. Bayes optimal template
584 matching for spike sorting - combining fisher discriminant analysis with optimal filtering. *Journal
585 of computational neuroscience*, 38, 439-459.
- 586 GHIASVAND, S., DUSSOURD, C. R., LIU, J., SONG, Y. & BERDICHEVSKY, Y. 2020. Variability of seizure-like
587 activity in an in vitro model of epilepsy depends on the electrical recording method. *Helicon*, 6,
588 e05587.
- 589 HELASSA, N., PODOR, B., FINE, A. & TOROK, K. 2016. Design and mechanistic insight into ultrafast
590 calcium indicators for monitoring intracellular calcium dynamics. *Sci Rep*, 6, 38276.
- 591 HU, X., KHANZADA, S., KLUTSCH, D., CALEGARI, F. & AMIN, H. 2022. Implementation of biohybrid
592 olfactory bulb on a high-density CMOS-chip to reveal large-scale spatiotemporal circuit
593 information. *Biosens Bioelectron*, 198, 113834.
- 594 INGEBRANDT, S. 2015. Sensing beyond the limit. *Nature Nanotechnology*, 10, 734-735.
- 595 JONATHAN W. PILLOW, M. S. 2019. Editorial overview: Machine learning, big data, and neuroscience.
596 *Current Opinion in Neurobiology*, 55, iii-iv.

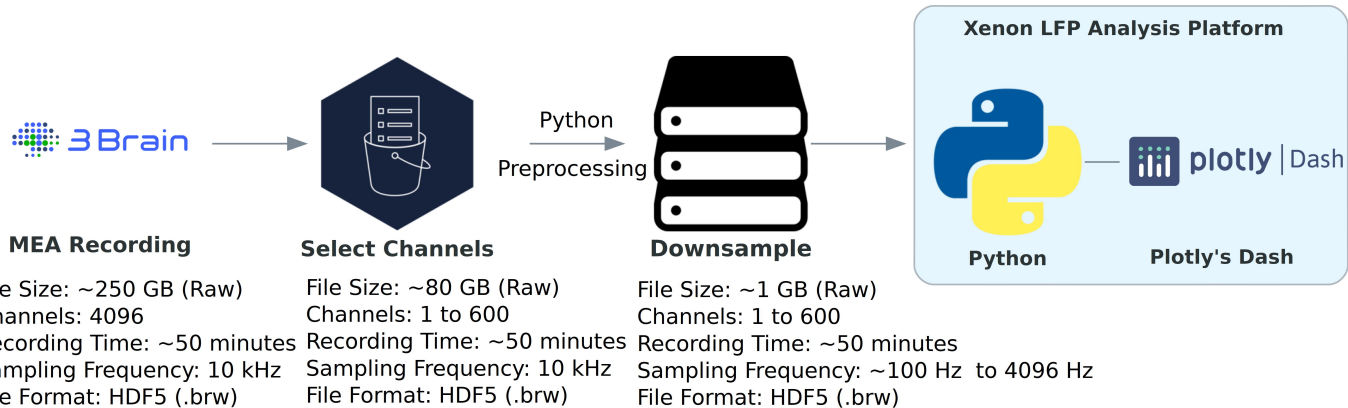
- 597 KULKARNI, R. U. & MILLER, E. W. 2017. Voltage Imaging: Pitfalls and Potential. *Biochemistry*, 56, 5171-
598 5177.
- 599 LANDHUIS, E. 2017. Neuroscience: Big brain, big data. *Nature*, 541, 559-561.
- 600 LEE, J., MITELUT, C., SHOKRI, H., KINSELLA, I., DETHE, N., WU, S., LI, K., REYES, E. B., TURCU, D., BATTY, E.,
601 KIM, Y. J., BRACKBILL, N., KLING, A., GOETZ, G., CHICHILNISKY, E. J., CARLSON, D. & PANINSKI, L.
602 2020. YASS: Yet Another Spike Sorter applied to large-scale multi-electrode array recordings in
603 primate retina. *bioRxiv*, 2020.03.18.997924.
- 604 LOPEZ, C. M., CHUN, H. S., WANG, S., BERTI, L., PUTZEYS, J., BULCKE, C. V. D., WEIJERS, J. W., FIRRINCIELI,
605 A., REUMERS, V., BRAEKEN, D. & HELLEPUTTE, N. V. 2018. A Multimodal CMOS MEA for High-
606 Throughput Intracellular Action Potential Measurements and Impedance Spectroscopy in Drug-
607 Screening Applications. *IEEE Journal of Solid-State Circuits*, 53, 3076-3086.
- 608 MACCIONE, A., GANDOLFO, M., ZORDAN, S., AMIN, H., DI MARCO, S., NIEUS, T., ANGOTZI, G. N. &
609 BERDONDINI, L. 2015. Microelectronics, bioinformatics and neurocomputation for massive
610 neuronal recordings in brain circuits with large scale multielectrode array probes. *Brain Res Bull*,
611 119, 118-26.
- 612 MACCIONE, A., HENNIG, M. H., GANDOLFO, M., MUTHMANN, O., VAN COPPENHAGEN, J., EGLEN, S. J.,
613 BERDONDINI, L. & SERNAGOR, E. 2014. Following the ontogeny of retinal waves: pan-retinal
614 recordings of population dynamics in the neonatal mouse. *J Physiol*, 592, 1545-63.
- 615 MACCIONE, A., SIMI, A., NIEUS, T., GANDOLFO, M., IMFELD, K., FERREA, E., SERNAGOR, E. &
616 BERDONDINI, L. Sensing and actuating electrophysiological activity on brain tissue and neuronal
617 cultures with a high-density CMOS-MEA. 2013 Transducers & Eurosensors XXVII: The 17th
618 International Conference on Solid-State Sensors, Actuators and Microsystems (TRANSDUCERS &
619 EUROSENSORS XXVII), 16-20 June 2013 2013. 752-755.
- 620 MACKENZIE-GRAY SCOTT, C., PARRISH, R. R., WALSH, D., RACCA, C., COWELL, R. M. & TREVELYAN, A. J.
621 2022. PV-specific loss of the transcriptional coactivator PGC-1alpha slows down the evolution of
622 epileptic activity in an acute ictogenic model. *J Neurophysiol*, 127, 86-98.
- 623 MAHMUD, M., BERTOLDO, A., GIRARDI, S., MASCHIETTO, M. & VASSANELLI, S. 2012. SigMate: a Matlab-
624 based automated tool for extracellular neuronal signal processing and analysis. *J Neurosci
Methods*, 207, 97-112.
- 626 MAHMUD, M. & VASSANELLI, S. 2016. Processing and Analysis of Multichannel Extracellular Neuronal
627 Signals: State-of-the-Art and Challenges. *Frontiers in Neuroscience*, 10.
- 628 MARTIN, M. S., DUTT, K., PAPALE, L. A., DUBE, C. M., DUTTON, S. B., DE HAAN, G., SHANKAR, A., TUFIK,
629 S., MEISLER, M. H., BARAM, T. Z., GOLDIN, A. L. & ESCAYG, A. 2010. Altered function of the
630 SCN1A voltage-gated sodium channel leads to gamma-aminobutyric acid-ergic (GABAergic)
631 interneuron abnormalities. *J Biol Chem*, 285, 9823-9834.
- 632 MEDRIHAN, L., FERREA, E., GRECO, B., BALDELLI, P. & BENFENATI, F. 2015. Asynchronous GABA Release
633 Is a Key Determinant of Tonic Inhibition and Controls Neuronal Excitability: A Study in the
634 Synapsin II-/- Mouse. *Cereb Cortex*, 25, 3356-68.
- 635 MICCOLI, B., LOPEZ, C. M., GOIKOETXEA, E., PUTZEYS, J., SEKERI, M., KRYLYCHKINA, O., CHANG, S.-W.,
636 FIRRINCIELI, A., ANDREI, A., REUMERS, V. & BRAEKEN, D. 2019. High-Density Electrical Recording
637 and Impedance Imaging With a Multi-Modal CMOS Multi-Electrode Array Chip. *Frontiers in
638 Neuroscience*, 13.
- 639 MISTRY, A. M., THOMPSON, C. H., MILLER, A. R., VANOEYE, C. G., GEORGE, A. L., JR. & KEARNEY, J. A.
640 2014. Strain- and age-dependent hippocampal neuron sodium currents correlate with epilepsy
641 severity in Dravet syndrome mice. *Neurobiol Dis*, 65, 1-11.
- 642 MOUČEK, R., BRŮHA, P., JEZEK, P., MAUTNER, P., NOVOTNY, J., PAPEZ, V., PROKOP, T., ŘONDÍK, T.,
643 ŠTĚBETÁK, J. & VAREKA, L. 2014. Software and hardware infrastructure for research in
644 electrophysiology. *Frontiers in Neuroinformatics*, 8.

- 645 MÜLLER, J., BALLINI, M., LIVI, P., CHEN, Y., RADIVOJEVIC, M., SHADMANI, A., VISWAM, V., JONES, I. L.,
646 FISCELLA, M., DIGGELMANN, R., STETTLER, A., FREY, U., BAKKUM, D. J. & HIERLEMANN, A. 2015.
647 High-resolution CMOS MEA platform to study neurons at subcellular, cellular, and network
648 levels. *Lab on a Chip*, 15, 2767-2780.
- 649 PACHITARIU, M., STEINMETZ, N., KADIR, S., CARANDINI, M. & KENNETH D., H. 2016. Kilosort: realtime
650 spike-sorting for extracellular electrophysiology with hundreds of channels. *bioRxiv*, 061481.
- 651 PANINSKI, L. & CUNNINGHAM, J. P. 2018. Neural data science: accelerating the experiment-analysis-
652 theory cycle in large-scale neuroscience. *Curr Opin Neurobiol*, 50, 232-241.
- 653 PARRISH, R. R., CODADU, N. K., MACKENZIE-GRAY SCOTT, C. & TREVELYAN, A. J. 2019. Feedforward
654 inhibition ahead of ictal wavefronts is provided by both parvalbumin- and somatostatin-
655 expressing interneurons. *J Physiol*, 597, 2297-2314.
- 656 PAULK, A. C., KFIR, Y., KHANNA, A. R., MUSTROPH, M. L., TRAUTMANN, E. M., SOPER, D. J., STAVISKY, S.
657 D., WELKENHUYSEN, M., DUTTA, B., SHENOY, K. V., HOCHBERG, L. R., RICHARDSON, R. M.,
658 WILLIAMS, Z. M. & CASH, S. S. 2022. Large-scale neural recordings with single neuron resolution
659 using Neuropixels probes in human cortex. *Nature Neuroscience*.
- 660 PERKEL, J. M. 2018. Data visualization tools drive interactivity and reproducibility in online publishing.
661 *Nature*, 554, 133-134.
- 662 PETER C. PETERSEN, J. H. S., NICHOLAS A. STEINMETZ, SARA MAHALLATI, GYÖRGY BUZSÁKI 2021.
663 CellExplorer: A framework for visualizing and characterizing single neurons. *Neuroresource*, 109,
664 3594 - 3608.
- 665 RAFIQ, A., GONG, Q. Z., LYETH, B. G., DELORENZO, R. J. & COULTER, D. A. 2003. Induction of prolonged
666 electrographic seizures in vitro has a defined threshold and is all or none: implications for
667 diagnosis of status epilepticus. *Epilepsia*, 44, 1034-41.
- 668 ROSSANT, C. 2016a. Moving away from HDF5. Available from: <https://cyrille.rossant.net/moving-away-hdf5/>.
- 669 ROSSANT, C. 2016b. Should you use HDF5? Available from: <https://cyrille.rossant.net/should-you-use-hdf5/>.
- 670 SEDAGHAT-NEJAD, E., FAKHARIAN, M. A., PI, J., HAGE, P., KOJIMA, Y., SOETEDJO, R., OHMAE, S.,
671 MEDINA, J. F. & SHADMEHR, R. 2021. P-sort: an open-source software for cerebellar
672 neurophysiology. *Journal of Neurophysiology*, 126, 1055-1075.
- 673 SEJNOWSKI, T. J., CHURCHLAND, P. S. & MOVSHON, J. A. 2014. Putting big data to good use in
674 neuroscience. *Nature Neuroscience*, 17, 1440-1441.
- 675 SOBOLEV, A., STOEWER, A., PEREIRA, M., KELLNER, C., GARBERS, C., RAUTENBERG, P. & WACHTLER, T.
676 2014. Data management routines for reproducible research using the G-Node Python Client
677 library. *Frontiers in Neuroinformatics*, 8.
- 678 STEINMETZ, N. A., ZATKA-HAAS, P., CARANDINI, M. & HARRIS, K. D. 2019. Distributed coding of choice,
679 action and engagement across the mouse brain. *Nature*, 576, 266-273.
- 680 STEVENSON, I. & KORDING, K. 2011. How advances in neural recording affect data analysis. *Nature
681 neuroscience*, 14, 139-42.
- 682 STREET, J. 2021. What advancements in clinical neurosciences need to occur in the next 10 years?
683 *Cambridge Medicine Journal*.
- 684 TAI, C., ABE, Y., WESTENBROEK, R. E., SCHEUER, T. & CATTERALL, W. A. 2014. Impaired excitability of
685 somatostatin- and parvalbumin-expressing cortical interneurons in a mouse model of Dravet
686 syndrome. *Proc Natl Acad Sci U S A*, 111, E3139-48.
- 687 TANG, S., REDDISH, F., ZHUO, Y. & YANG, J. J. 2015. Fast kinetics of calcium signaling and sensor design.
688 *Curr Opin Chem Biol*, 27, 90-7.

- 691 TOADER, O., FORTE, N., ORLANDO, M., FERREA, E., RAIMONDI, A., BALDELLI, P., BENFENATI, F. &
692 MEDRIHAN, L. 2013. Dentate gyrus network dysfunctions precede the symptomatic phase in a
693 genetic mouse model of seizures. *Front Cell Neurosci*, 7, 138.
694 TREVELYAN, A. J., SUSSILLO, D. & YUSTE, R. 2007. Feedforward inhibition contributes to the control of
695 epileptiform propagation speed. *J Neurosci*, 27, 3383-7.
696 VANWALLEGHEM, G., CONSTANTIN, L. & SCOTT, E. K. 2020. Calcium Imaging and the Curse of Negativity.
697 *Front Neural Circuits*, 14, 607391.
698 WEI, Z., LIN, B. J., CHEN, T. W., DAIE, K., SVOBODA, K. & DRUCKMANN, S. 2020. A comparison of
699 neuronal population dynamics measured with calcium imaging and electrophysiology. *PLoS*
700 *Comput Biol*, 16, e1008198.
701 XIAO, S., LOWET, E., GRITTON, H. J., FABRIS, P., WANG, Y., SHERMAN, J., MOUNT, R. A., TSENG, H. A.,
702 MAN, H. Y., STRAUB, C., PIATKEVICH, K. D., BOYDEN, E. S., MERTZ, J. & HAN, X. 2021. Large-scale
703 voltage imaging in behaving mice using targeted illumination. *iScience*, 24, 103263.
704 XIN HU, S. K., DIANA KLÜTSCH, FEDERICO CALEGARI, HAYDER AMIN, 2022. Implementation of biohybrid
705 olfactory bulb on a high-density CMOS-chip to reveal large-scale spatiotemporal circuit
706 information Biosensors and Bioelectronics. *Biosensors and Bioelectronics*, 198.
707 YGER, P., SPAMPINATO, G. L. B., ESPOSITO, E., LEFEBVRE, B., DENY, S., GARDELLA, C., STIMBERG, M.,
708 JETTER, F., ZECK, G., PICAUD, S., DUEBEL, J. & MARRE, O. 2018. A spike sorting toolbox for up to
709 thousands of electrodes validated with ground truth recordings in vitro and in vivo. *eLife*, 7,
710 e34518.

711

High Density Multi-Electrode Array LFP Activity Data Analysis Pipeline



Xenon LFP Analysis Platform

Input File Path:

C:/User/Desktop/Example-Slice.brw

SUBMIT

Select Image File:

Drag and Drop or [Select File](#)

File Path
C:/User/Desktop/

File Name
Example-Slice.brw

Active Channels
407

Data per Channel
898952

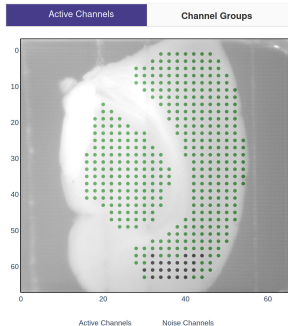
Recording Time (Seconds)
2997

Sampling (Hz)
300

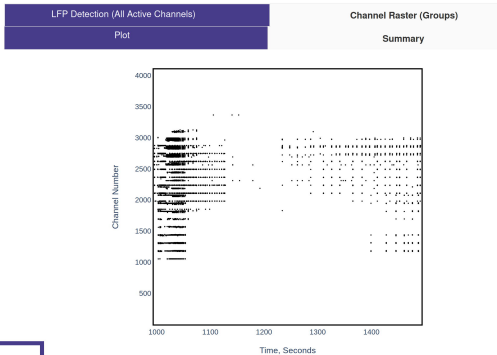
Select a Time Range for Analysis:



Select Channels for Plots



LFP Raster Plots



Analysis Settings

LFP Detection Channel Raster

Digital Filter Parameters:

Lower Cut-Off Frequency: 0
Upper Cut-Off Frequency: 100

Turn-ON-Filter

Butterworth
 Chebyshev

LFP Parameters:

Threshold (mV): 0.07
Time duration (Seconds): 0.02

Upward Peak Only
 Upward & Downward Peak

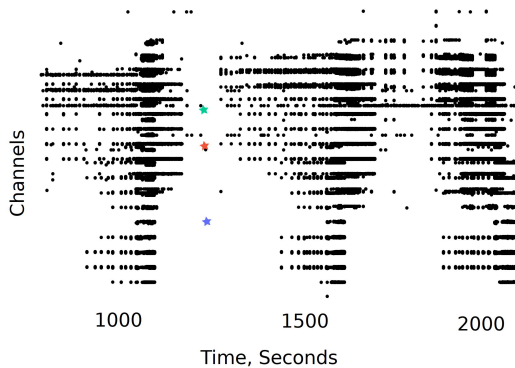
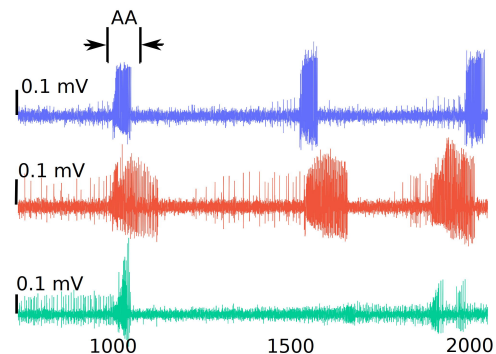
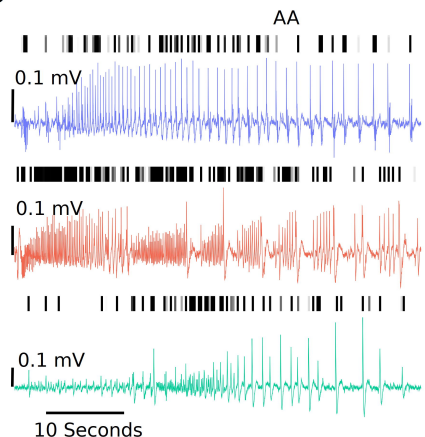
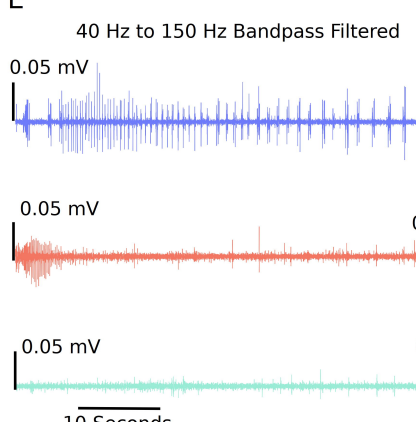
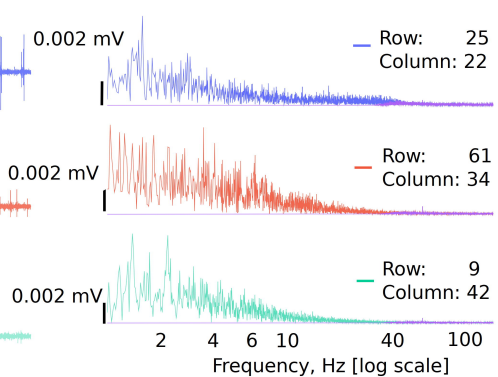
Multi-Channel Select & View

- Full time trace with interactive zoom
- Frequency transformation (FFT)
- Detect and highlight channels with potential noise
- Image & picture overlay
- Select groups of channels for analysis

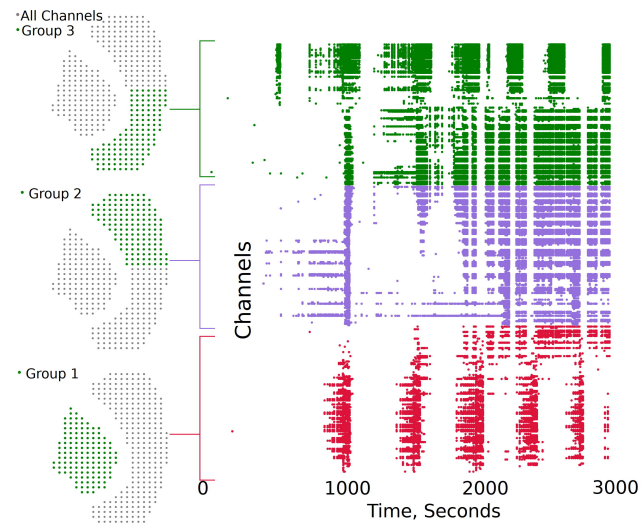
Time Range Selection for analysis

- Select time range for large data files
- Generate LFP activity and raster plots

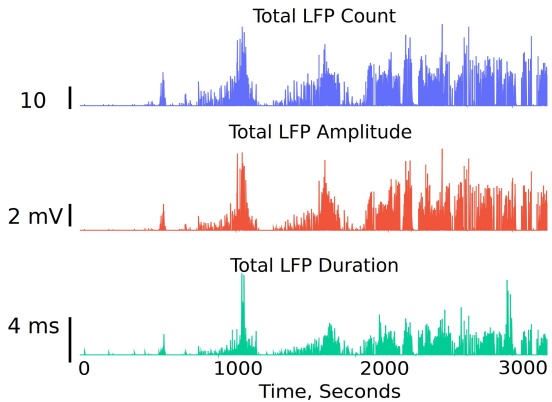
- Summary plots, group raster and measures
- Low pass, high pass, band pass digital filtering

A**B****C****D****E****F**

A



B



Group	Total LFP Count (count/s)	Total Channels	Active Channels	LFP Count [Top 20] (count/s)	Mean Amplitude [Top 20] (mV)	Mean Duration [Top 20] (s)
1	4.99	132	83	3.14	0.153	0.047
2	4.94	142	105	1.9	0.145	0.087
3	6.51	133	88	3.62	0.096	0.062

A Time-series trace

Row: 29
Column: 20

0.1 mV

B Short-time Fourier Transform

0.04 mV

C LFP Activity



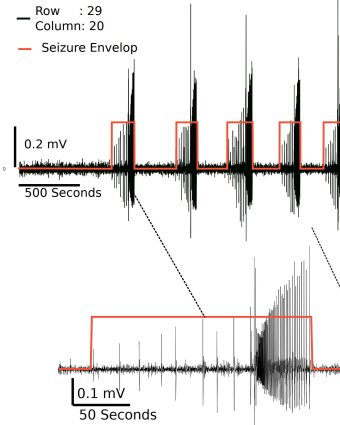
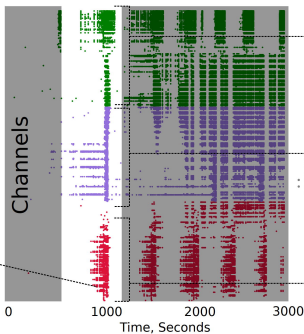
D Spectral activity



E Seizure-like activity envelop

500 s



A**B****C**